Tribology International 189 (2023) 108976

Contents lists available at ScienceDirect

Tribology International

journal homepage: www.elsevier.com/locate/triboint

Experimental comparison of the transition speed of a hydrodynamic journal bearing lubricated with oil and magnetorheological fluid

G.H.G. van der Meer [a,*], F. Quinci [b], W. Litwin [c], M. Wodtke [c], R.A.J. van Ostayen [a]

[a] Delft University of Technology, Department of Precision and Microsystems Engineering, Mekelweg 2, Delft, 2628 CD, The Netherlands
[b] Bifröst Research and Development B.V., Molenvliet 34, Wijk bij Duurstede, 3961 MW, The Netherlands
[c] Gdansk University of Technology, Faculty of Mechanical Engineering and Ship Technology, Narutowicza 11/12, Gdansk 80-233, Poland

ARTICLE INFO

Keywords:
Magnetorheological lubrication
Friction
Stribeck curve
Finite Element Method

ABSTRACT

A journal bearing test bench is used to find the transition speed between the hydrodynamic and mixed lubrication regimes for a modified magnetorheological (MR) fluid. It is shown that the transition speed of the bearing can be reduced by applying a local magnetic field near minimum film when it is lubricated with the MR fluid, and that this will only marginally increase friction. The lubricating performance of the MR fluid is compared to that of a reference oil, and all experimental results are compared with a Finite Element model based on the Reynolds equation.

1. Introduction

Hydrodynamic journal bearings are used to support high speed rotating shafts through a thin film of pressurised lubricant, separating the bearing surfaces and reducing friction and wear [1,2]. This pressure generation is the result of the relative motion between the shaft and bearing, and scales with the speed of the shaft. At low speeds the pressure generation will be insufficient to carry the load, causing a transition from the high speed hydrodynamic lubrication regime to the low speed mixed or even boundary lubrication regime. In applications where the shaft frequently has to start and stop, this not only increases power consumption, but can reduce the lifetime of the bearing as well due to increased wear. For those applications it is desired to reduce the transition speed, the minimum speed where the bearing can still operate in the hydrodynamic regime, as much as possible.

Several methods exist for improving the low speed performance of hydrodynamic journal bearings. One effective way of separating the surfaces is by using a hydrostatic or hybrid bearing, where at low speeds the oil film is created with high pressure lubricant provided by an external pump [3]. This allows for low friction operation of the bearing at all speeds, however, if the pump were to fail the performance of the bearing would deteriorate, causing an unexpected increase in friction and wear. Another technique that can be used to increase pressure generation and load capacity at all speeds is the use of textured surfaces. However, these are susceptible to wear during boundary lubrication and can be difficult to design correctly, leading to a decrease in performance if the operating conditions are unfavourable [4,5]. A third technique, which is also the focus of this research, is the use of so-called 'smart' lubricants that experience a change in rheological properties when exposed to an external field [6].

One of these smart lubricants are the magnetorheological (MR) fluids. An MR fluid consists of a mineral carrier oil with a large concentration of iron microparticles in suspension, usually amounting to about 70 to 80% of the total mass, as well as a number of additives [7]. When a magnetic field is applied to the fluid the particles will interact and form structures. These structures trap the oil and have the effect of turning the fluid into a viscoplastic solid at low shear stresses, while at higher shear stresses the structures are partially broken apart, leading to a higher effective viscosity that scales with increasing magnetic field strength. When the magnetic field is removed, the particles lose their magnetisation and the structures dissipate within a few milliseconds, returning the viscosity to its original value [8–10].

Due to the complicated non-Newtonian behaviour of these fluids, there exists a large amount of literature focused on developing analytical or numerical models [11]. For a lubricated contact using MR fluid, this can be done with a continuum approach which requires the use of one of several rheological models. Generally, either the Bingham plastic or Herschel–Bulkley model is used, but multiple other models exist as well [11,12]. Both models include the viscoplastic behaviour of an MR fluid at low shear stress using a yield stress that depends on the magnetic field strength. Above the yield stress, the Bingham plastic assumes a linear relation between shear stress and shear rate, while the Herschel–Bulkley model also includes the effects of shear-thinning. Shear-thinning should be taken into account when the shear

* Corresponding author.
E-mail address: G.H.G.vanderMeer@tudelft.nl (G.H.G. van der Meer).

https://doi.org/10.1016/j.triboint.2023.108976
Received 27 July 2023; Received in revised form 1 September 2023; Accepted 23 September 2023
Available online 27 September 2023

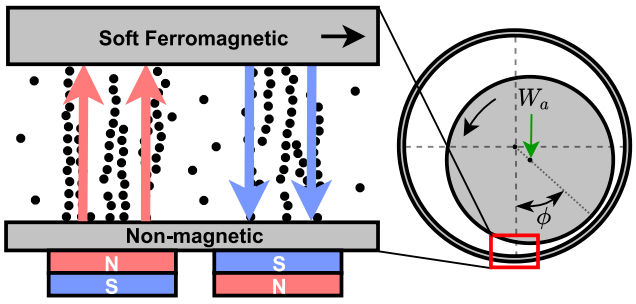

Fig. 1. A schematic figure (not to scale) of an MR-lubricated journal bearing with a local magnetic field applied just before the location of minimum film. The magnetic field moves from the left magnet to the shaft, and then through the shaft and back to the magnet on the right. This figure is just for illustration, the actual magnetic field that was used during the experiments is discussed in Section 2.3.

rate is high (order of magnitude $> 1 \times 10^4$ s^{-1}) [13,14], which is generally the case in high speed hydrodynamic journal bearings. For modelling a bearing lubricated with an MR fluid, the rheological model is usually combined with either the Navier–Stokes equations [15,16], or the Reynolds equation [17,18], which is a simplified form of the Navier–Stokes equations that can be used for thin film flows [19].

On the experimental side, MR fluids have been used most successfully in active dampers [20], even resulting in some commercial applications [21,22]. However, the use of these fluid in bearings has also gotten some attention, although it should be noted that only a limited number of experimental investigations could be found in literature. Hesselbach and Abel-Keilhack [23] used MR lubrication in a hydrostatic bearing with the aim of achieving a constant bearing gap for variable load. By varying the magnetic field at constant load they could obtain large changes in gap size with relatively small magnetic fields. Based on these findings, they concluded that very high stiffness could be achieved in a closed-loop system with a constant bearing gap, which was later attempted experimentally in [24]. A hydrodynamic journal bearing lubricated with MR fluid was investigated by Urreta et al. [25], who found that for the same configuration of magnetic coils, a magnetisable carbon steel shaft resulted in higher load capacity and a more stable locus than a non-magnetic stainless steel shaft. They mention that this increase in load capacity could be used to widen the operating range of a hydrodynamic bearing, reducing the transition speed. Bompos and Nikolakopoulos [26] looked at the stability of oil and MR-lubricated rotor systems, and found that compared to oil lubrication the activated MR fluid increased stiffness and damping, while reducing the diameter of the shaft orbits at low load. Vaz et al. [27] found experimentally that the high viscosity of activated MR fluid not only increases load capacity, but also friction force. Several numerical investigations also cite this as the main drawback of MR lubrication [15,16,28].

This friction force increase of MR fluid compared to standard lubricant is problematic, since it will increase the power consumption of the system. A promising method of limiting the friction increase while still increasing load capacity might be to locally magnetise the MR lubricant film (see Fig. 1), instead of magnetising the entire film as is usually done [29]. Quinci et al. [30] tested this concept experimentally and compared it with oil lubrication, but still recorded high friction losses for the MR fluid. They did note that the standard commercial MR fluid that was used was not optimal for their specific application, and had a very high base and magnetised viscosity compared to the base viscosity of the oil and MR fluid. They suggested creating an MR fluid tailor-made for hydrodynamic lubrication.

In summary, literature demonstrates that MR fluid can be used as a lubricant in hydrodynamic journal bearings in order to increase the load capacity, which at low speeds results in a reduction of the transition speed. However, the main drawback is the increased friction coefficient compared to standard lubricant due to the higher viscosity of MR fluids [15,16,27,28]. While it has been suggested [29,30] that it might be possible to reduce the friction coefficient with MR lubrication by locally magnetising the film and by optimising the MR fluid to decrease its viscosity, the experimental verification of this hypothesis does not yet exist. Therefore, this paper presents for the first time in literature the experimental and numerical results of a hydrodynamic journal bearing lubricated with a locally magnetised low viscosity MR fluid. Our research shows that this approach will indeed result in less friction than when using a reference lubricant, without the loss of the magnetically induced load capacity increase at low speeds.

Table 1
Overview of the bearing properties and operating conditions.

Property	Symbol	Value
Shaft diameter	D	50 mm
Bearing length	L	100 mm
Nominal radial clearance	h_0	100 μm
Bearing surface roughness	Ra	0.4 μm
Shaft surface roughness	Ra	0.4 μm
Lubrication groove radius/length		1 mm/50 mm
Moment arm length		200 mm
Rotational speed	n	0 to 500 rpm
Applied load/Specific pressure	W_a/p_m	2.5 kN/0.5 MPa
Average lubricant temperature	T	32 °C
Lubricant pump flow rate	Q_{in}	0.3 L min^{-1}
Magnet remanence	B_r	1.29-1.32 T
Magnets diameter/length		20 mm/20 mm
Centre-to-centre distance magnets	L1	20.8 mm
Distance magnets-film	L2	8 mm

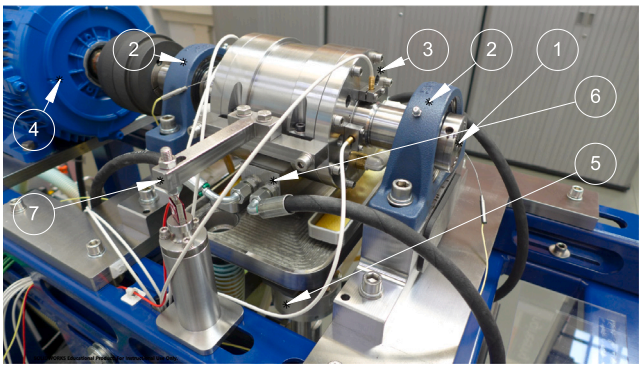

Fig. 2. The setup used to conduct the measurements. 1 — main shaft, 2 — support bearings, 3 — bearing housing, 4 — electric motor, 5 — load cell, 6 — hydrostatic bearing, 7 — moment arm.

2. Materials and methods

The experimental measurements in this research were performed using a custom-built setup for testing a hydrodynamic journal bearing. With standard mineral oil lubrication (from now on the "reference measurements") and MR lubrication (from now on the "MR measurements") the shaft locus, coefficient of friction and bearing temperature were measured for different speeds, with the aim of identifying the transition speed of the bearing system. These experimental results were compared with the numerical results from a model based on the 2D Reynolds equation. This section provides the details of the setup and experimental procedure, as well as the lubricant properties and the structure of the numerical model.

2.1. Experimental setup

A photo of the experimental setup is shown in Fig. 2, the main properties of the setup and experimental conditions can be found in

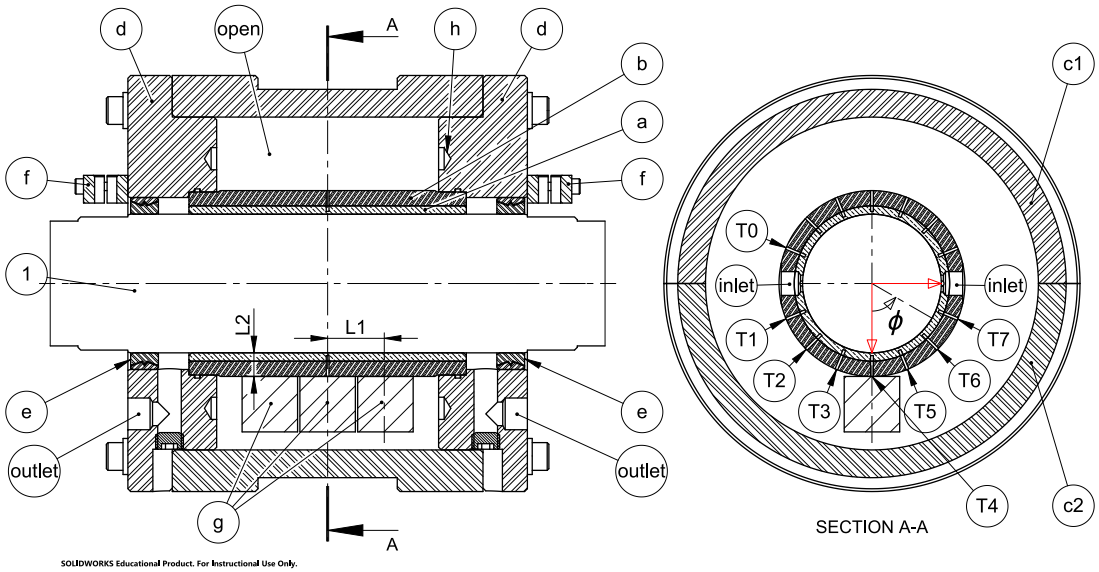

Fig. 3. Schematic cross-section of the bearing housing. 1 — main shaft, a — bearing bush, b — reinforcement bush, c1&c2 – housing shells, d — housing flanges, e — labyrinth seals, f — capacitive sensor clamps, g — permanent neodymium magnets, h — notch, T0-T7 — thermocouples. The coordinate system that was used is shown in the cross-section on the right, the shaft rotates in the positive ϕ direction. Not shown is the non-magnetic 3D-printed structure that fills the space marked with 'open' and is used to keep the magnets in place. This structure is fixed in the housing using the four notches.

Table 1. The setup consists of a 50 mm shaft (1) supported by two self-aligning ball bearings (2), with the housing that contains the hydrodynamic journal bearing (3) centred in between the ball bearings. The shaft is driven by a 5.5 kW AC electric motor (4) that is controlled via a frequency inverter, with velocity feedback provided by an incremental encoder mounted on the shaft inside the motor housing. A pneumatic jack is used to generate a constant radial load, which is measured with a Futek LCF455 load cell (5) mounted on the piston (accuracy about ±30 N), and can be changed by modifying the air pressure in the jack. The jack is mounted on a small shaft parallel to the main shaft (1) which is supported by two ball bearings, to prevent it from constraining the movement of the housing around the main shaft. A hydrostatic bearing (6) supplied by a hydraulic pump then transfers the load from the jack to the bearing housing, creating a hydrostatic oil film in between those two components. This allows for accurate friction measurements using a moment arm and a 100 lb Futek LSB201 load cell (7). Following the data sheet [31] and assuming rectangular probabilities, this load cell has a standard combined uncertainty of ±0.39 N. The friction force in the bearing is determined from these measurements by calculating the bearing torque (multiplying the load cell force with the distance between the load cell and the centre line of the bearing) and dividing it by the bearing radius. Assuming an applied load of 2.5 kN, this translates to a standard deviation on the measured friction coefficient of ±0.0012. The uncertainty due to the dimensional tolerances of the housing and moment arm were found to be negligible compared to the uncertainty of the sensor, and were therefore not included in the final calculation. The lubricant of the hydrodynamic bearing (oil or MR fluid) is pumped from a reservoir with a separate cavity pump, a positive displacement type pump selected for its ability to pump fluids with high particle content. The bearing is connected to the pump with flexible silicon tubes to limit the influence of the tubes on the friction measurement.

2.1.1. Overview of the bearing

A schematic overview of the bearing housing is shown in Fig. 3. Permanent magnets were used to locally magnetise the MR fluid, and one of the main considerations during the design of the bearing housing was that it should be possible to create any magnetic pattern in the film, without replacing or moving the bearing bush. For that reason, only the edges of the bearing bush (a & b) are used to support it in the C45 steel flanges (d) of the housing. The resulting open space (marked with 'open' in the figure) can be utilised to place the permanent magnets in any desired pattern using disposable 3D-printed support structures (not shown). To limit deformations of the relatively soft bronze bearing bush (a) due to the hydrodynamic pressure buildup in the bearing, it is press-fitted inside a stiffer AISI 304 steel bush (b). The housing is completed with two half-cylindrical C45 steel shells (c1 & c2), which can be removed to access the magnets while the bearing is installed on the shaft. As a result, it is only necessary to remove the bearing from the shaft in order to clean it when switching lubricants.

Lubricant enters the bearing through two inlet holes at $\phi = 90°$ and $\phi = -90°$ ($\phi = 0°$ is the rest position of the shaft, see Fig. 3 for the coordinate system), with a groove distributing the lubricant in the axial direction. The lubricant exits the bearing at both axial ends where it can return to the reservoir. Aluminium contactless labyrinth seals (e) are used to reduce leakage, these were selected to prevent the seals from affecting the friction measurement. The bearing sleeve temperature was measured using eight 1 mm OD type K thermocouples (accuracy about ±1.5 K) installed in radially drilled holes 2 mm below the bearing inner surface, with one additional thermocouple measuring fluid temperature inside one of the two inlets (not shown). The expected temperature of the fluid film will probably be slightly higher than the temperature measured by the thermocouples. However, taking into account the high thermal conductivity of the bronze bearing sleeve and the relatively light operating conditions of the test, it is expected that the difference between the fluid film and sleeve temperatures will be small. Finally, two Micro-Epsilon capaNCDT6200 amplifiers control four Micro-Epsilon CS05 capacitive distance sensors (accuracy about ±0.15 μm, sensors not shown), that are mounted on the housing using clamps (f) to measure the locus of the shaft. Two sensors are installed 90° apart on either side of the housing, the locus is determined by averaging the results from both sides.

2.2. Lubricant properties

For the reference measurements Castrol MHP 153 (SAE 30) was used, which is a lubricating oil designed specifically for maritime applications (such as stern tube bearing lubrication). The MR measurements were performed using a modified version of the commercially available MR fluid MRHCCS4-A designed by Liquids Research Ltd. At request,

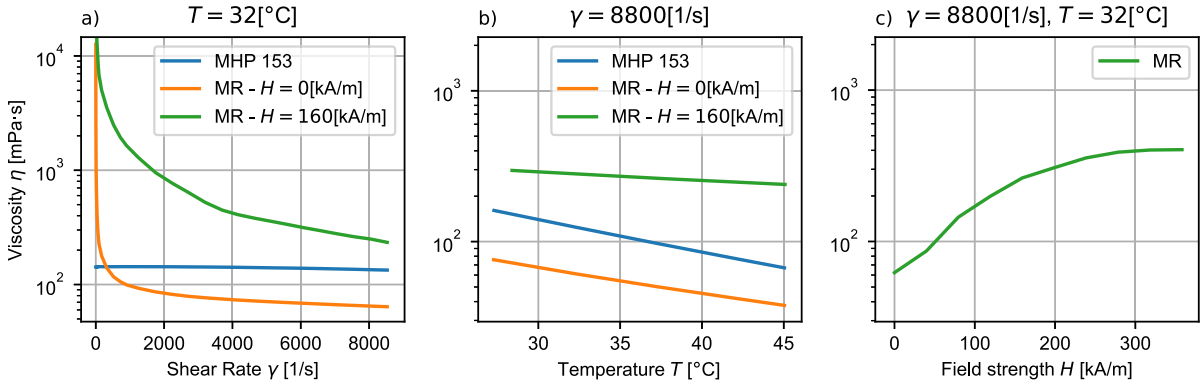

Fig. 4. (a) Effective viscosity vs shear rate for both lubricants and different magnetic fields (constant temperature). (b) Effective viscosity vs temperature for both lubricants and different magnetic fields (constant shear rate). (c) Effective viscosity vs magnetic field strength for the MR lubricant (constant temperature and shear rate). Take note that only subfigures (b) and (c) use the same scale for the y-axis.

the commercial fluid was modified by Liquids Research Ltd. to reduce the viscosity of the MR fluid to below that of the reference oil at high shear rates. In addition, the mass fraction of the 1 to 2 μm particles was reduced from 70 to 20%, and the ratios of the various additives were modified. The effective viscosity of both the MR and reference lubricants was validated for different shear rates and temperatures using an Anton Paar MRC 302 rheometer with a cone type spindle. The viscosity of the MR fluid was also measured with magnetic fields of different strength applied. The results are shown in Fig. 4.

Fig. 4a clearly shows the strong shear thinning properties of the MR fluid, especially compared to the standard lubricant (which is also slightly shear-thinning). When a magnetic field is applied, the viscosity of the MR fluid increases rapidly, especially at lower shear rates. However, shear rates in the bearing are expected to be relatively high (order of magnitude 1×10^4 s^{-1}), at which point the MR viscosity without magnetic field is about half that of the reference lubricant. With a magnetic field of 160 kA m^{-1} the viscosity at high shear rates is increased approximately by a factor 2, and it is clear that the shear-thinning effect becomes stronger. For comparison, the unmodified MR fluid is only 10% less viscous than the reference lubricant at high shear rates, and its viscosity increases by a factor 7 when magnetised at 160 kA m^{-1}. At low shear rates the difference between the modified and unmodified MR fluid is even larger. At 1000 s^{-1} the viscosity of the modified MR fluid increases by a factor 15 when a 160 kA m^{-1} magnetic field is applied, while the viscosity of the unmodified MR fluid increases by a factor 40. Fig. 4b shows that both the standard lubricant and the MR fluid show a decrease in viscosity for an increase in temperature. With the magnetic field activated this decrease becomes less strong, because the influence of the magnetised particle structures on the viscosity starts dominating the influence of the carrier oil [32]. Finally, Fig. 4c shows the magnetic response of the MR lubricant. Here it can be seen that at higher magnetic field strengths the particles reach saturation, causing the curve to flatten out.

2.2.1. Bearing sleeve temperature

The viscosity measurements with varying shear rate and varying field strength were both performed at constant temperature of 32 °C. This temperature was chosen based on the film temperatures measured by the thermocouples during the Stribeck measurements, Fig. 5 shows some representative temperature profiles. Please take into account that no heat exchanger was used to keep the lubricant reservoir at a constant temperature during the measurements.

Fig. 5a shows the bearing sleeve temperature profiles in the lower right quadrant of the bearing at high speed (n = 500 rpm) for both the reference and MR measurements (see Fig. 3 for the thermocouple locations). For all lubricants, the variation in film temperatures inside the bearing is seen to be small, the variation is less than 1 °C. Fig. 5b shows the temperature over time in thermocouple T7, again for both measurements. Here it can be seen that the temperature in the oil-lubricated bearing mostly stabilises after about 1000 s, while the temperature in the MR-lubricated bearings continues to rise during the Stribeck measurements, leading to a temperature increase of slightly less than 3 °C over the course of the experiment. It is not known why the temperature does not stabilise during the time frame of the test when using MR lubrication, but it might be related to the different thermal properties the two fluids, as well as the different amounts of fluid in the reservoir (see Section 2.4).

2.3. Magnetic field properties

For the MR measurements with magnetic field, a relatively simple magnetic pattern was used. Based on some simple initial numerical calculations, three cylindrical N42 neodymium magnets were placed in a line along the axial direction at an angle of $\phi = 0°$ as can be seen in Fig. 7a. Because the bearing bush is non-magnetic, a fairly uniform magnetic field is formed locally between the magnets and the steel shaft. Furthermore, it was found that by reversing the polarity of the central magnet with respect to the other two, the field strength in the rest of the film could be reduced even further.

The resulting magnetic field was calculated with the "Magnetic Fields, No Currents (mfnc)" interface of the AC/DC module of the commercial FEM software package COMSOL Multiphysics® 6.1. This interface implements Gauss' law for the magnetic field using the scalar magnetic potential, with cubic order shape functions. The 3D computational domain can be seen in Fig. 6, only one quarter of the system is modelled since it is symmetric. The parts that are highlighted in the figure (C45 housing and shaft) are assumed to be soft ferromagnetic and are modelled with a magnetisation curve (curve data taken from measurements in [33]). The influence of the housing on the magnetic field in the film was found to be relatively minor (especially close to the magnets), which is why the housing geometry was simplified by removing all internal features (inlets, outlets, bolt holes, etc...) in order to reduce the computational complexity of the problem. All other parts are assumed to be non-magnetic and have a relative permeability of 1 (air domain), or are not modelled (bearing bush). The permanent magnets are modelled with the remanent flux density magnetisation model (see Table 1 and Fig. 7 for magnet strength and orientation respectively). An unstructured tetrahedral mesh was generated for the computational domain using the "extremely fine" mesh preset, resulting in a mesh with 158 733 elements with a quadratic order shape function. The standard solver (Newton–Raphson iteration with under-relaxation) was used with a relative tolerance of 1×10^{-3} in order to calculate the solution for a total of 731 371 degrees of freedom. These settings were confirmed by a mesh convergence study.

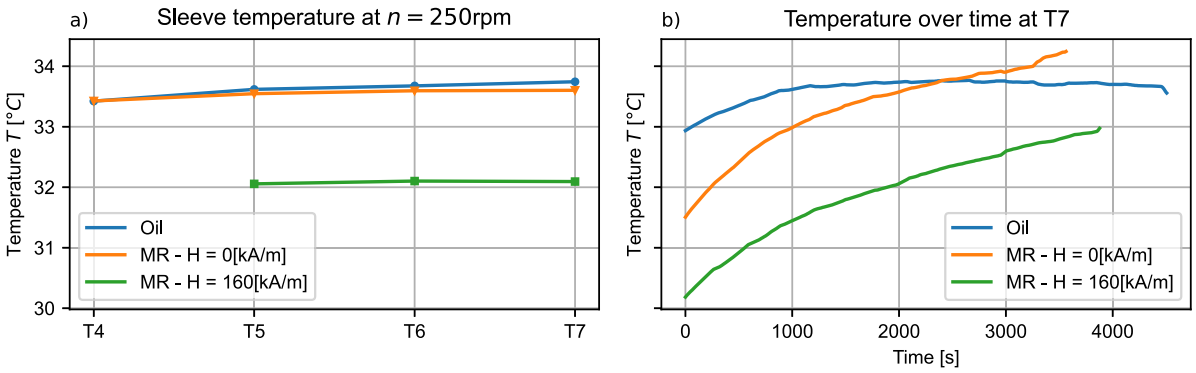

Fig. 5. (a) The bearing sleeve temperature near minimum film for all lubricants. The temperature profiles are shown for only one speed per lubricant (250 rpm corresponds to $t = 2100$ s), these results are representative of the profiles at all speeds. Thermocouple T4 is missing for the measurement with activated MR fluid, since a permanent magnets was placed at that location instead. (b) Sleeve temperature over time for the different lubricants as measured by thermocouple T7, which recorded the highest temperatures of all thermocouples.

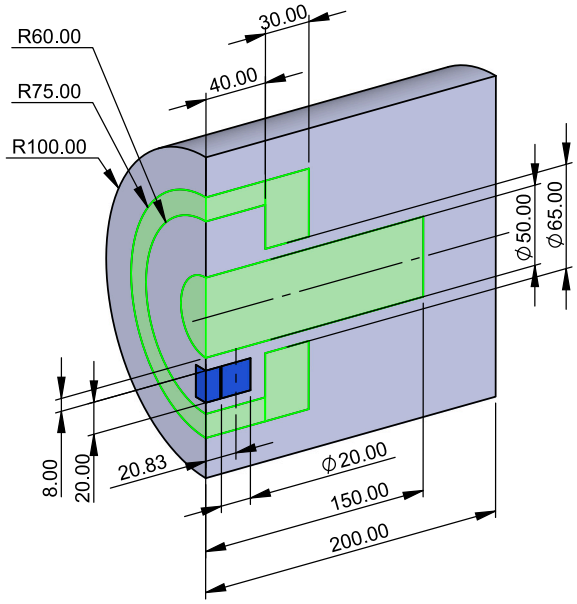

Fig. 6. The 3D computational domain used to calculate the magnetic field in the fluid film. The soft ferromagnetic shaft and housing are highlighted in green, the magnets in dark blue, and the air in grey. Dimensions are in millimetres.

Fig. 7b shows a profile of the magnetic field strength in the middle of the film (the change in magnetic field strength over the film thickness is negligible), where it is clear that the strongest magnetic field is located around $\phi = 0$, and that the magnetic field is negligibly small almost everywhere else. There is a small increase in magnetic field strength near the edges of the bearing ($y = 0$ & $y = 1$) where it is supported by the (ferromagnetic) steel flanges of the housing, but this effect is small as well.

2.4. Experimental procedure

All measurements were performed under identical experimental conditions, only changing the lubricant or the magnetic field depending on the measurement being conducted. The goal of these measurements was to identify the critical transition speed where the bearing changes from the hydrodynamic regime to the mixed or boundary lubrication regime, which was done by generating Stribeck curves at a constant load (2.5 kN/0.5 MPa).

Before every single Stribeck measurement, the setup was warmed up by letting it run at the target load and at maximum speed (500 rpm) until the lubricant temperature in the tank reached 26 °C. Depending on the lubricant, the ambient conditions, and the volume of lubricant in the tank, this took anywhere between 1 and 3 h. The lubricant volume was 7 L for the standard lubricant, but due to its high cost only 1.5 L of the MR fluid were used at a time.

After the warm up, the Stribeck measurement was conducted by reducing the speed from 500 to 300 rpm in steps of 50 rpm, and then from 300 to 0 rpm in steps of 25 rpm. After every step the speed was kept constant for 5 min to allow for stabilisation of the temperature in the film. If at any point during this test, the coefficient of friction (CoF) became larger than 0.02 for more than 1 min, the bearing was assumed to have entered mixed or boundary lubrication and the measurement was stopped. During every step, LabVIEW was used to read data from all sensors at a frequency of 100 Hz, apart from the thermocouples which were read at 3 Hz. For the final 10 s of every step, data from the capacitive sensors was read 500 times per shaft revolution (e.g., 1875 Hz at 225 rpm) to enable an accurate calculation of the shaft locus.

Finally, after the Stribeck curve had been recorded the clearance circles were measured (without removing the applied load) to be able to place the shaft locus in the bearing [34]. This means that the capacitive sensors were used to record the maximum clearance of the shaft in the bearing for all angular coordinates ϕ, by rotating the bearing housing 360° around the shaft. For this process, the moment arm and tubing were removed, and only the hydrostatic bearing was left turned on. The clearance circle was then constructed by least-squares fitting a circle through 12 points recorded by the capacitive sensors at evenly spaced angles.

2.5. Numerical modelling

The hydrodynamic performance of the bearing in the experimental setup has also been compared with a FEM numerical model made using COMSOL® Multiphysics 6.1 [35]. The aim was to compare the reference measurements with a numerical model validated in literature, and to see if this model could correctly predicted the trends of the MR measurements in the hydrodynamic regime. The mixed and/or boundary lubrication regimes are not included in the model, which means that the transition speed cannot be determined exactly. The model that was used is based on 2D Reynolds equation combined with the JFO boundary conditions to include cavitation. Because the difference in temperature in the film was found to be small during the experiments (as discussed in Section 2.2.1), it was assumed that an effective (constant) film temperature of 32 °C could be used, which is the average film temperature over time for all measurements. The effect of shear-thinning on the viscosity was not taken into account either. The reasoning for this is that the shear thinning effect of the MR fluids (especially without magnetic field) is less pronounced at the

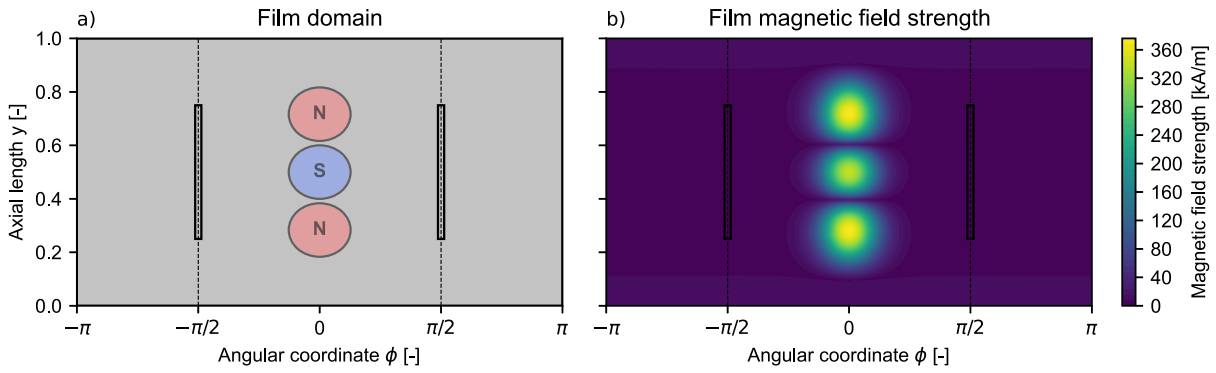

Fig. 7. (a) The unfolded fluid film of the journal bearing, with the magnets and inlets shown at respectively $\phi = 0$ and $\phi = -\pi/2 \& \phi = \pi/2$. The distance (out-of-plane) between the magnet surface and the film is 8 mm, the pole that is turned towards the film is indicated with 'N' (north) or 'S' (south). (b) The corresponding norm of the magnetic field strength profile in the fluid film in kA m^{-1}. The profile is taken at the middle of the film.

relatively high shear rates expected to be found in the bearing. At shear rates close to zero shear-thinning is much stronger, and MR yield stress would also have to be taken into account. In the current model the viscosity at a shear rate of $\gamma = 8800\ \mathrm{s}^{-1}$ is used for all speeds, as well as the magnetic field dependency from Fig. 4c.

Eq. (1) shows the Reynolds equation as found in [36], with pressure p, cavitation mass fraction f_c, film thickness h, viscosity η and shaft surface speed u. In order to include cavitation, a variable transformation is used to replace both p and f_c with functions of a new variable ξ (Eqs. (2) & (3)). By assuming that at any point in the computational domain, the lubricant is either in a full film region ($p > 0$, $f_c = 1$) or in a cavitated region ($p = 0$, $f_c < 1$), the Reynolds equation can be solved for a single variable (ξ) that represents either the pressure or the mass fraction, depending on its sign.

$$\frac{\partial}{\partial x}\left(-\frac{h^3 f_c}{12\eta}\frac{\partial p}{\partial x} + \frac{h f_c u}{2}\right) + \frac{\partial}{\partial y}\left(-\frac{h^3 f_c}{12\eta}\frac{\partial p}{\partial y}\right) = 0 \tag{1}$$

$$p = (\xi \geq 0)\xi \tag{2}$$

$$f_c = 1 + (\xi < 0)c_f \xi \tag{3}$$

By entering Eqs. (2) & (3) in the Reynolds equation, and by adding artificial diffusion in the x- and y-directions using the transformation constant c_f ($c_f = h^2/(3\eta h_e)$ with mesh element size h_e), the Reynolds equation is reduced to Eq. (4). For a detailed derivation and discussion of this cavitation algorithm, and the calculation of the transformation constant, the reader is referred to [36].

$$\frac{\partial}{\partial x}\left(-\frac{h^3}{12\eta}\frac{\partial \xi}{\partial x} + \frac{h f_c u}{2}\right) + \frac{\partial}{\partial y}\left(-\frac{h^3}{12\eta}\frac{\partial \xi}{\partial y}\right) = 0 \tag{4}$$

The implementation of the model is extended in a two ways. First of all, the steady state shaft locus is determined by solving Eqs. (5) and (6) for the film pressure p, with F_x and F_y the horizontal and vertical load capacities respectively.

$$F_x = \iint_S p \sin\phi \mathrm{d}A = 0 \tag{5}$$

$$F_y = \iint_S p \cos\phi \mathrm{d}A = W_a \tag{6}$$

The second extension is a simple equation for calculating the inlet pressure p_{in}. Since a positive displacement pump is used for transporting the lubricant, it is not possible to assume a constant inlet pressure for all speeds of the shaft, like with a pressure-driven flow. Instead, the flow coming out of the pump (with volume flow rate Q_{in}) will be divided over inlets 1 and 2 (with volume flow rates Q_1 and Q_2), with the ratio Q_1/Q_2 being a function of the speed. This is modelled with equation (7), which is solved for p_{in}.

$$Q_1 + Q_2 - Q_{in} = 0 \tag{7}$$

The volume flow rates Q_1 and Q_2 are obtained by integrating the flow rates q_x and q_y (from the continuity equation) over the boundaries of the inlets.

Finally, the friction coefficient f is determined using equation (8), with the integrand evaluated at the stationary surface. This surface corresponds to the inner surface of the hydrodynamic bearing, which is connected to the moment arm used for measuring friction in the experimental setup (number 7 in Fig. 2).

$$f = \frac{\iint \tau_{xz}\big|_{z=0} \mathrm{d}A}{W_a} \tag{8}$$

2.5.1. Software implementation

The Reynolds equation (Eq. (4)) is implemented as a General Form PDE in COMSOL® with cubic order Lagrangian shape functions, and Eqs. (5)–(7) are added as global equations. The pressure is set to 0 (atmospheric pressure) at the open edges of the bearing ($y = 0$ and $y = 1$) using a Dirichlet boundary condition, and similarly the pressure at the edges of the inlet is set to the value of p_{in} with a Dirichlet boundary condition as well. A periodic boundary condition is used for the edges of the computational domain at $x = -\pi$ and $x = \pi$. The computational domain (shown in Fig. 7a) is discretised using a structured quad mesh with a maximum element size equal to the diameter of the inlet grooves, resulting in 3950 quad elements and a total of 35 941 degrees of freedom to be solved for. The solution process uses a segregated solver that is based on Newton–Raphson iteration with under-relaxation and is assumed to be converged when the relative tolerance is lower than 1×10^{-6}. During the solution process the first step is to calculate an initial solution by solving the Reynolds equation individually (without Eqs. (5)–(7)) at the maximum speed of 500 rpm. After that all four equations are solved at the same time, and a parameter sweep is used to reduce the speed in steps of 25 rpm. The sweep is set to stop once the speed reaches the transition speed that was found experimentally, the transition speed is not calculated by the model. All of these settings were confirmed to give mesh convergence.

3. Results and discussion

In this section the results of the reference measurements with oil, and the MR measurements with and without magnetic field are presented and discussed. All three sets of measurements were performed four times under the same operating conditions, with the figures in this

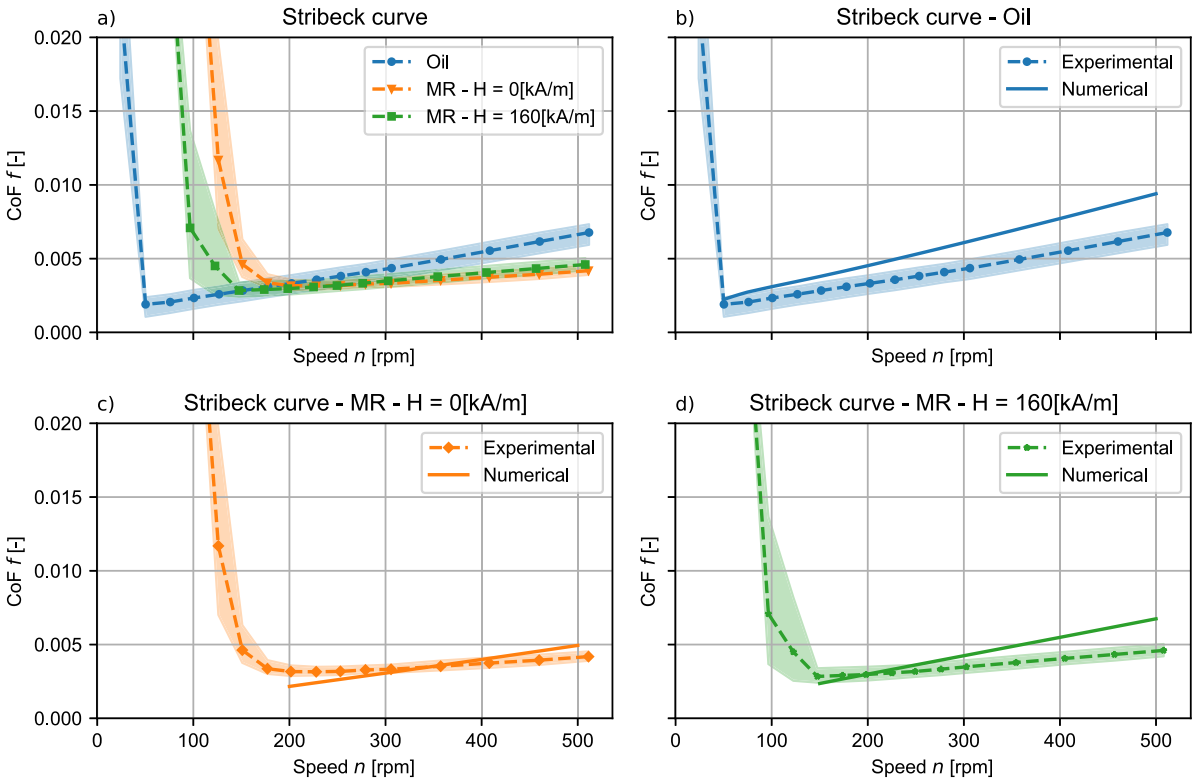

Fig. 8. (a) Experimental Stribeck curves for the reference and MR measurements, showing the difference in transition speed between the tests. The maximum and minimum friction values recorded during the repeated measurements are indicated by the shaded regions, while the average value is indicated by the dotted line. (b–d) The experimental Stribeck curves together with the numerically calculated friction coefficients in the hydrodynamic regime (solid lines), shown respectively for (b) oil lubrication, (c) MR lubrication without magnetic field and (d) MR lubrication with a magnetic field.

section showing the average of those four repetitions for the Stribeck curve and the shaft locus (including eccentricity and attitude angle plots).

3.1. Stribeck curve

The experimental and numerical Stribeck curves as a function of shaft rpm are shown in Fig. 8 for the reference and MR measurements. The experimental curves in Fig. 8a show good repeatability, especially in the hydrodynamic regime where the error margins are approximately equal in size for all lubricants. These error margins show the maximum and minimum friction values that were recorded during the four repetitions, and looking at all measurements the largest difference is less than 0.0014 (for the reference measurement). In the mixed regime the differences between the repeated measurements are much larger, which could be related to the stochastic nature of mixed lubrication. The transition between the hydrodynamic and mixed regimes is well-defined for the reference measurement, but it is much more gradual for the MR measurements. This could be explained by the presence of the particles in the MR fluid, which have varying diameters. When the speed of the shaft is decreased, at first only the largest particles will cause contact between the bearing and the shaft, but when the speed is lowered further this will occur more and more often and for smaller particles. This could lead to the gradual friction increase observed in the experiments.

Looking at the data in more detail, it is clear that the oil-lubricated reference bearing displays the lowest transition speed at around 50 rpm (with the transition speed defined as the speed where the coefficient of friction (CoF) is minimal). However, while the MR measurements with and without magnetic field show a substantial transition speed increase compared to the reference measurement, the transition speed of the MR measurement with a magnetic field present is lower than that of the measurement without magnetic field. The difference in transition speed is about 50 rpm, or a decrease of about 25% going from around 200 rpm without magnetic field to around 150 rpm with field. This clearly shows that the applied magnetic pattern from Fig. 7 successfully increases the load capacity of the bearing at low speeds, although it should be noted that even then, the transition speed of the oil-lubricated reference bearing is around 66% lower still.

When examining the CoF in the hydrodynamic regime, however, something interesting can be seen. Starting at speeds larger than about 225 to 250 rpm, the CoF of both of the MR measurements drops below the CoF from the reference measurements. At 500 rpm, this results in an average CoF of 0.0047 for MR-lubrication with magnetic field, which is almost 30% lower than the average of 0.0065 recorded with oil lubrication. At higher speeds, this difference will become even larger. Meanwhile, the effect on the CoF of applying the magnetic field to the MR-lubricated bearing is limited, resulting in an average increase of only 14% compared to the situation without magnetic field.

The explanation for why the MR measurements show increased transition speeds and decreased CoFs is simple. As can be seen in Fig. 4, the base viscosity of the MR fluid (at high shear rates) is about half that of the standard lubricant. Lubricating a bearing with a lower viscosity lubricant results in a lower load capacity (and therefore a higher transition speed), but also in lower friction, which is exactly what is being shown by the current results. This explanation is confirmed by the numerical results in Fig. 8b, which were calculated using the viscosity data from Fig. 4 and show the same trends. In fact, the fluid viscosity was the only difference between the simulations for oil lubrication and MR lubrication without magnetic field, which are shown in Figs. 8b and 8c respectively. There are some deviations between the friction values in the simulations and experiments, specifically, at high speeds the simulations seem to predict larger friction values than were found experimentally. This can likely be attributed to the Newtonian and isothermal approximations that were used during the simulations, but this will be discussed in more detail in Section 3.2.

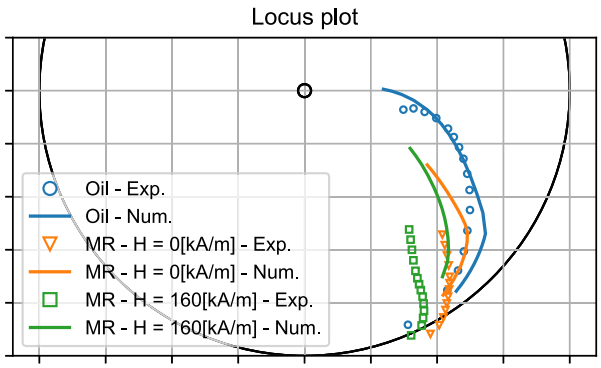

Fig. 9. The experimental (Exp.) and numerical (Num.) shaft loci for the reference and MR measurements. The small black circle indicates the centre of the bearing, the larger black circle indicates the inner bearing surface.

The results that were obtained could not have been achieved with a standard commercial MR fluid. Prior research on hydrodynamic lubrication with these fluids has generally concluded that while they increase load capacity, the increase in friction can be quite high and is generally undesirable [15,16,37]. Furthermore, the friction issue is exacerbated by the fact that most often the entire fluid film is magnetised. By locally magnetising the film, additional parameters controlling the shape, strength, and position of the magnetic pattern are introduced, which can be tweaked to influence both the load capacity and friction changes [29,30]. Combine this with a lower viscosity MR fluid with fewer particles (described in Section 2.2), and the current research shows that the result can be an MR-lubricated bearing that experiences less friction (at high speeds in the hydrodynamic regime) than its oil-lubricated counterpart, while still allowing for a transition speed decrease through the application of a magnetic field. It should also be noted that the specific modified MR fluid and magnetic pattern used in this research could still be optimised further. For example, by increasing the viscosity (base, magnetised, or both) of the MR fluid, or by increasing the strength and magnetised area of the magnetic pattern, it might be possible to create an MR-lubricated bearing that has both a lower transition speed than, and lower or comparable friction to, a bearing lubricated with mineral oil.

3.2. Shaft locus

Next to the friction coefficient, the experimental and numerical shaft loci were also obtained for both the reference and MR measurements, as shown in Fig. 9. The shaft locus (the position of the shaft inside the bearing) is plotted as a function of the shaft speed, and for all measurements the points closest to the bearing centre correspond to the highest speed (n = 500 rpm), while the points on the clearance circle correspond to speeds at or below the transition speed. The locus gives an indication of the film thickness for a specific speed, the closer it is to the centre of the bearing, the thicker the film.

Looking at the experimental results, the shaft locus measurements make sense considering the friction coefficient results discussed in the previous section. The higher viscosity mineral oil used for the reference measurements resulted in a lower transition speed due to an increased load capacity, which translates to thicker films compared to MR lubrication. This can also be seen in Fig. 10, which shows that for all speeds, the eccentricity is lower with oil lubrication. Similarly, comparing the MR measurements with and without magnetic field shows that applying the magnetic field also lowers the eccentricity, again corresponding to the transition speed decrease seen in Fig. 8.

The same general trends are shown by the numerical results. The agreement between experiment and simulation is quite good for the reference measurement, with the numerical locus roughly following the same path as the experimental locus. The numerical model does predict lower eccentricities, especially at higher speeds, which might be caused by the isothermal approximation for the fluid film as was mentioned in the last section. If thermal effects were taken into account, the higher heat generation at higher speeds would results in lower viscosities and therefore higher eccentricities and lower friction values. The accuracy of the model is less good for the MR measurements, with the model underpredicting eccentricity and overpredicting attitude angle, but the general trend of higher eccentricity and lower attitude angle for MR lubrication (compared to oil lubrication) can still be seen. The larger deviations of the numerical model for the MR measurements are not surprising, since the model does not take shear-thinning into account, which is much more important for MR fluid than for oil as can be seen in Fig. 4. Taking this non-Newtonian effect into account would likely result in lower viscosity near the region of minimum film, where the shear rate is relatively high due to the small film thickness. The overall effect would then be a lower load capacity, and likely a better match with the experimental results.

One thing of note in the locus plot, is that the simulation predicts an attitude angle larger than 90° for oil lubrication at the highest speed of 500 rpm. This seems to be related to the combination of a relatively low load (2.5 kN/0.5 MPa), together with the positive displacement pump that supplies a constant flow of lubricant to the two inlets at 90° and −90°. Due to the constant flow rate, the numerical model predicts a relatively high inlet pressure, and for the highest speed this pressure is even similar in value to the film pressure at minimum film. This is likely the cause of the relatively high attitude angles, since modelling the bearing with constant pressure inlets that provide oil at ambient pressure, results in attitudes angles well below 90°. While it is known that a high speed, lightly loaded bearing operating close to 90° can suffer from unstable whirling of the shaft [1,38], this was not observed during any of the measurements.

An attempt was made to perform measurements at higher loads as well (1 – 2 MPa), but it was quickly discovered that this resulted in severe wear to the bearing, even after only one or two Stribeck measurements at these loads. This wear resulted in a groove in axial direction near the location of minimum film with a depth of up to 10 μm, which was enough to noticeably modify the shape of the locus at low speeds. For this reason, these results were discarded. The damage was likely caused by abrasive wear due to the presence of the iron microparticles in the contact zone, which is a known phenomenon [39,40]. This would also explain why the eccentricity at low speed became slightly larger than 1 for both MR measurements (Fig. 10a). Apparently, even at the relatively low load of 0.5 MPa that was used during the tests, some wear did build up over the course of multiple separate Stribeck measurements with MR lubrication, resulting in a small groove. This phenomenon is currently being investigated by the authors.

4. Conclusion

The current research has shown experimentally that it is possible to lubricate a hydrodynamic journal bearing with a magnetorheological (MR) fluid, and at the same time obtain friction values lower than that of the reference oil lubricated bearing. This was done without losing the capability to reduce the transition speed of the MR-lubricated bearing by applying a local magnetic field near minimum film. This is in contrast to literature, where it is generally reported that MR-lubricated bearings have much lower transition speeds, but also much larger friction values due to the high viscosity of MR fluids. The results in this research were obtained by locally magnetising the fluid film, and by lubricating the bearing with a modified version of a commercial MR fluid with reduced particle content and lowered base viscosity. This modified MR fluid is also less viscous (without magnetic field) than the reference oil that was tested, explaining why the oil lubricated bearing has a lower transition speed, but also experiences more friction. These results were confirmed by the numerical finite element model

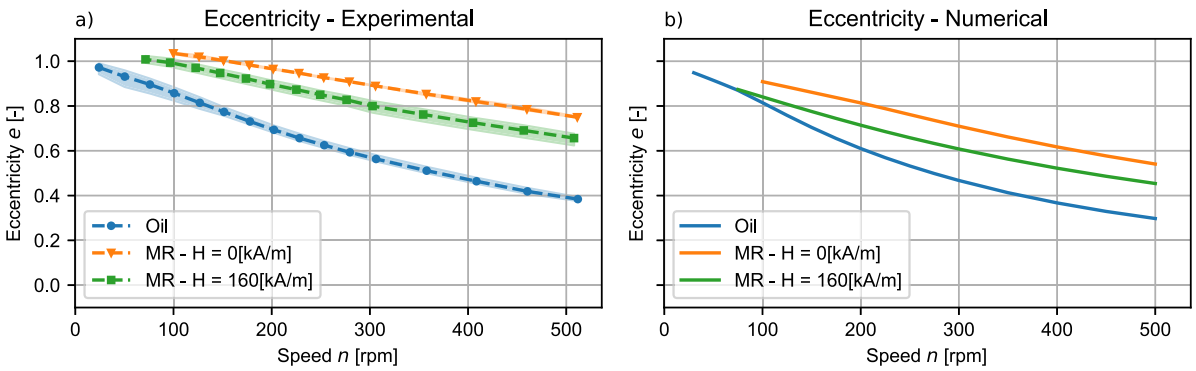

Fig. 10. The (a) experimental and (b) numerical eccentricity values for the reference and MR measurements. In subfigure a, the maximum and minimum eccentricity values recorded during the repeated measurements are indicated by the shaded regions, while the average value is indicated by the dotted line.

made in COMSOL® Multiphysics, which predicts the same trends as were observed in the experiments. The accuracy of this model could further be improved by taking shear thinning into account using the generalised Reynolds equation.

Overall, it can be concluded that MR fluid lubrication of journal bearings does not necessarily have to increase the friction coefficient of the bearing. The next step would therefore be to try and find a combination of an MR fluid and a localised magnetic field that results in both a lowered transition speed and a minimal friction increase, combining the benefits of the traditional MR fluids with a strong magnetic response and the modified MR fluid with lower viscosity.

CRediT authorship contribution statement

G.H.G. van der Meer: Methodology, Software, Validation, Investigation, Data curation, Writing – original draft, Visualisation. **F. Quinci:** Conceptualisation, Investigation, Resources, Writing – review & editing, Supervision, Funding acquisition. **W. Litwin:** Investigation, Writing – review & editing. **M. Wodtke:** Investigation, Writing – review & editing. **R.A.J. van Ostayen:** Conceptualisation, Writing – review & editing, Supervision, Funding acquisition.

Declaration of competing interest

The authors declare that they have no known competing financial interests or personal relationships that could have appeared to influence the work reported in this paper.

Data availability

Data will be made available on request.

Acknowledgments

The research work was inspired and financed by Bifröst Research and Development B.V., The Netherlands company as a part of an R&D department effort on the development of modern-type bearings.

References

[1] Stachowiak GW, Batchelor AW. Engineering tribology, vol. 9780521609. Butterworth-Heinemann; 2005, p. 1–488. http://dx.doi.org/10.1017/CBO9780511805905.
[2] van Beek A. Advanced engineering design lifetime performance and reliability. TU Delft; 2010.
[3] Rowe W. Hydrostatic, aerostatic and hybrid bearing design. Butterworth-Heinemann; 2013, p. 352. http://dx.doi.org/10.1016/C2011-0-07331-3.
[4] Gachot C, Rosenkranz A, Hsu SM, Costa HL. A critical assessment of surface texturing for friction and wear improvement. Wear 2017;372–373:21–41. http://dx.doi.org/10.1016/j.wear.2016.11.020.
[5] Gropper D, Wang L, Harvey TJ. Hydrodynamic lubrication of textured surfaces: A review of modeling techniques and key findings. Tribol Int 2016;94:509–29. http://dx.doi.org/10.1016/j.triboint.2015.10.009.
[6] Michalec M, Svoboda P, Krupka I, Hartl M. Tribological behaviour of smart fluids influenced by magnetic and electric field – A review. Tribol Ind 2018;40(4):515–28. http://dx.doi.org/10.24874/ti.2018.40.04.01.
[7] Ashtiani M, Hashemabadi SH, Ghaffari A. A review on the magnetorheological fluid preparation and stabilization. J Magn Magn Mater 2015;374:711–5. http://dx.doi.org/10.1016/j.jmmm.2014.09.020.
[8] Bossis G, Volkova O, Lacis S, Meunier A. Magnetorheology: Fluids, structures and rheology. In: Odenbach S, editor. Ferrofluids: Magnetically controllable fluids and their applications. Berlin, Heidelberg: Springer Berlin Heidelberg; 2002, p. 202–30. http://dx.doi.org/10.1007/3-540-45646-5_11.
[9] de Vicente J, Klingenberg DJ, Hidalgo-Alvarez R. Magnetorheological fluids: A review. Soft Matter 2011;7(8):3701–10. http://dx.doi.org/10.1039/c0sm01221a.
[10] Kumar S, Sehgal R, Wani MF, Sharma MD. Stabilization and tribological properties of magnetorheological (MR) fluids: A review. J Magn Magn Mater 2021;538:168295. http://dx.doi.org/10.1016/j.jmmm.2021.168295.
[11] Ghaffari A, Hashemabadi SH, Ashtiani M. A review on the simulation and modeling of magnetorheological fluids. J Intell Mater Syst Struct 2015;26(8):881–904. http://dx.doi.org/10.1177/1045389X14546650.
[12] Zubieta M, Eceolaza S, Elejabarrieta MJ, Bou-Ali MM. Magnetorheological fluids: Characterization and modeling of magnetization. Smart Mater Struct 2009;18(9). http://dx.doi.org/10.1088/0964-1726/18/9/095019.
[13] Becnel AC, Hu W, Wereley NM. Measurement of magnetorheological fluid properties at shear rates of up to 25000 s -1. IEEE Trans Magn 2012;48(11):3525–8. http://dx.doi.org/10.1109/TMAG.2012.2207707.
[14] Farjoud A, Vahdati N, Fah YF. Mathematical model of drum-type MR brakes using herschel-bulkley shear model. J Intell Mater Syst Struct 2008;19(5):565–72. http://dx.doi.org/10.1177/1045389X07077851.
[15] Bompos DA, Nikolakopoulos PG. CFD simulation of magnetorheological fluid journal bearings. Simul Model Pract Theory 2011;19(4):1035–60. http://dx.doi.org/10.1016/j.simpat.2011.01.001.
[16] Gertzos KP, Nikolakopoulos PG, Papadopoulos CA. CFD analysis of journal bearing hydrodynamic lubrication by Bingham lubricant. Tribol Int 2008;41(12):1190–204. http://dx.doi.org/10.1016/j.triboint.2008.03.002.
[17] Dorier C, Tichy J. Behavior of a Bingham-like in lubrication flows. J Non-Newton Fluid Mech 1992;45(3):291–310. http://dx.doi.org/10.1016/0377-0257(92)80065-6.
[18] Lampaert SG, van Ostayen RA. Lubrication theory for Bingham plastics. Tribol Int 2020;147:106160. http://dx.doi.org/10.1016/j.triboint.2020.106160.
[19] Hamrock BJ. Fundamentals of fluid film lubrication. 2nd ed. CRC Press; 2004, p. 728. http://dx.doi.org/10.1201/9780203021187.
[20] Rahman M, Ong ZC, Julai S, Ferdaus MM, Ahamed R. A review of advances in magnetorheological dampers: their design optimization and applications. J Zhejiang Univ Sci A 2017;18(12):991–1010. http://dx.doi.org/10.1631/jzus.A1600721.
[21] Jolly MR, Bender JW, Carlson JD. Properties and applications of commercial magnetorheological fluids. J Intell Mater Syst Struct 1999;10(1):5–13. http://dx.doi.org/10.1177/1045389x9901000102.
[22] Zhu X, Jing X, Cheng L. Magnetorheological fluid dampers: A review on structure design and analysis. J Intell Mater Syst Struct 2012;23(8):839–73. http://dx.doi.org/10.1177/1045389X12436735.
[23] Hesselbach J, Abel-Keilhack C. Active hydrostatic bearing with magnetorheological fluid. J Appl Phys 2003;93(10 3):8441–3. http://dx.doi.org/10.1063/1.1555850.
[24] Guldbakke JM, Hesselbach J. Development of bearings and a damper based on magnetically controllable fluids. J Phys Condens Matter 2006;18(38):S2959. http://dx.doi.org/10.1088/0953-8984/18/38/S29.

[25] Urreta H, Leicht Z, Sanchez A, Agirre A, Kuzhir P, Magnac G. Hydrodynamic bearing lubricated with magnetic fluids. J Intell Mater Syst Struct 2010;21(15):1491–9. http://dx.doi.org/10.1177/1045389X09356007.
[26] Bompos DA, Nikolakopoulos PG. Experimental and analytical investigations of dynamic characteristics of magnetorheological and nanomagnetorheological fluid film journal bearing. J Vib Acoust Trans ASME 2016;138(3). http://dx.doi.org/10.1115/1.4032900.
[27] Vaz N, Binu KG, Serrao P, Hemanth MP, Jacob J, Roy N, et al. Experimental investigation of frictional force in a hydrodynamic journal bearing lubricated with magnetorheological fluid. J Mech Eng Autom 2017;7(5):131–4. http://dx.doi.org/10.5923/J.JMEA.20170705.01.
[28] Bhat AK, Vaz N, Kumar Y, D'Silva R, Kumar P, Binu KG. Comparative study of journal bearing performance with ferrofluid and MR fluid as lubricant. AIP Conf Proc 2019;2080(1). http://dx.doi.org/10.1063/1.5092926.
[29] Lampaert SG, Quinci F, van Ostayen RA. Rheological texture in a journal bearing with magnetorheological fluids. J Magn Magn Mater 2020;499:166218. http://dx.doi.org/10.1016/j.jmmm.2019.166218.
[30] Quinci F, Litwin W, Wodtke M, van den Nieuwendijk R. A comparative performance assessment of a hydrodynamic journal bearing lubricated with oil and magnetorheological fluid. Tribol Int 2021;162(April):107143. http://dx.doi.org/10.1016/j.triboint.2021.107143.
[31] Futek model LSB201 data sheet. 2023, https://media.futek.com/content/futek/files/pdf/productdrawings/lsb201.pdf. [Accessed 24 August 2023].
[32] Hemmatian M, Sedaghati R, Rakheja S. Temperature dependency of magnetorheological fluids' properties under varying strain amplitude and rate. J Magn Magn Mater 2020;498. http://dx.doi.org/10.1016/j.jmmm.2019.166109.
[33] Liu X, Shi Z, Mo N, Zhao J, Yang G. Calculation and experiment of electromagnetic force of the axial AMB used in HTR-PM main helium blower prototype and its dual material selection method. Appl Comput Electromagn Soc J 2019;34(4):584–90.
[34] Litwin W. Experimental research on marine oil-lubricated stern tube bearing. Proc Inst Mech Eng J 2019;233(11):1773–81. http://dx.doi.org/10.1177/1350650119846004.
[35] COMSOL AB. COMSOL multiphysics® version 6.1. 1986-2023, https://www.comsol.com/.
[36] Alakhramsing S, van Ostayen R, Eling R. Thermo-hydrodynamic analysis of a plain journal bearing on the basis of a new mass conserving cavitation algorithm. Lubricants 2015;3(2):256–80. http://dx.doi.org/10.3390/lubricants3020256.
[37] Laukiavich CA, Braun MJ, Chandy AJ. A comparison between the performance of ferro- and magnetorheological fluids in a hydrodynamic bearing. Proc Inst Mech Eng J 2014;228(6):649–66. http://dx.doi.org/10.1177/1350650114523753.
[38] Nicolas JC. Hydrodynamic journal bearings - Types characteristics and applications. In: Mini course notes, 20th annual meeting, vibration institute, no. July. 1996, p. 81–100, URL https://dyrobes.com/wp-content/uploads/2016/04/Hydrodynamic-Journal-Bearings-Types-Characteristics-and-Applications_linked.pdf.
[39] Leung WC, Bullough WA, Wong PL, Feng C. The effect of particle concentration in a magneto rheological suspension on the performance of a boundary lubricated contact. Proc Inst Mech Eng J 2004;218(4):251–63. http://dx.doi.org/10.1243/1350650041762622.
[40] Wong PL, Bullough WA, Feng C, Lingard S. Tribological performance of a magneto-rheological suspension. Wear 2001;247(1):33–40. http://dx.doi.org/10.1016/S0043-1648(00)00507-X.